

Optimal interlayer structure for information spreading on multilayer networks

Liming Pan,¹ Wei Wang,^{2,*} Shimin Cai,¹ and Tao Zhou¹

¹Web Sciences Center, School of Computer Science and Engineering,
University of Electronic Science and Technology of China, Chengdu, 611731, China

²Cybersecurity Research Institute, Sichuan University, Chengdu 610065, China

(Dated: May 23, 2019)

Many real-world systems ranging from social, biological to infrastructures can be modeled by multilayer networks. Promoting information spreading on multilayer networks has significant contributions in conducting advertisements for e-commercial products and predicting popular scientific publications. In this paper, we propose an optimal strategy to promote spreading via adding one interconnecting edge between two isolated networks. Basing on a perturbation theory of the discrete Markovian chain approach, we deviate an index that evaluating the spreading prevalence in the interconnected network approximately. The index can be interpreted as a variant of Katz centrality, with edges weighted by the dynamical information of the spreading process. Those weights will enhance the edges that lowly infected in one end and its neighborhood, while highly infected in the other. We verify the effectiveness of the strategy on small networks by exhaustively examining all latent edges and find it gives optimal or close to optimal performance. For large synthetic and real world networks, it always outperforms some other heuristic strategies like connecting nodes with highest degrees or eigenvector centralities.

I. INTRODUCTION

Promoting information spreading is a hot topic in the field of network science, statistical physics and computer science [1]. When information is spreading on networked systems, how to maximize the spreading prevalence is of both theoretical and practical importance. The strategies for achieving better spreading can be roughly divided into three categories, including identifying the vital nodes [2–14], designing effective transmission strategies [15–20] and network structural perturbations [21–24]. For vital nodes identification, centrality measures, e.g. K-core, H-index, betweenness and degree-based centralities, are assigned to nodes of networks. Nodes with high centralities are then chosen to be initial seeds. For effective transmission strategies, spreading protocols are designed to avoid invalid contacts (i.e., contacts among infected nodes). For structural perturbation methods, structures of the networks are modified slightly in order to achieve better spreading [21]. Structural perturbation is also widely applied to enhance the synchronizability of the networks [25–29].

Previous studies have revealed that spreading dynamics on multilayer networks can be fundamentally different from that on single layer networks [30–38]. For instance, Granell *et al.* [32] found that the epidemic spreading has a metacritical point that defined by the awareness dynamics and the topology of multilayer networks. The structure of interconnections between two networks has indelible effects on the robustness [39–42], synchronization [25, 43] and spreading dynamics [44–46]. Saumell-Mendiola *et al.* [47] showed that interlayer degree correlations can benefit epidemic outbreak. When considering coevolution of epidemic and information spreading on multilayer networks, Wang *et al.* [34] revealed that the interlayer degree correlations can also suppress the epidemic outbreak without altering the outbreak threshold.

Understanding what is a better interlayer structure is important to understand the dynamics on multilayer networks and for designing more effective systems. To address this problem, Aguirre *et al.* [21] applied a matrix perturbation approach, and found that adding a connection between two hubs is more likely to promote the spreading dynamics for two competing networks. Until recently, Pan *et al.* [48] suggested a perturbation theory for the adjacency matrix to obtain the optimal interconnections between two networks. The method works near the spreading threshold when a small number of edges are added.

In this paper, we develop a theoretical framework that gives optimal or close to optimal interconnecting edge for all parameter regions. Starting with the discrete Markovian chain approach when the two networks are isolated, we develop a perturbation theory which gives the spreading prevalence in the interconnected network approximately. Then the edge with top approximate spreading prevalence is chosen as the optimal edge. This approximate prevalence incorporates information of both network structure and dynamics. It also has a very simple physical interpretation as Katz centrality of edges weighted by the information of dynamics.

In what follows, we present the descriptions of the model in Sec. II, and then develop a theory to obtain the optimal interconnecting strategy in Sec. III. We perform extensive numerical simulations to verify the effectiveness of our strategy in Sec. IV. Finally, in Sec. V we draw conclusions.

II. MODEL DESCRIPTIONS

In this paper, we consider information spreading on two-layered networks. Let the subnetwork of two layers be a and b respectively, the number of nodes in network a (b) is denoted by N_a (N_b) and number of edges M_a (M_b). The adjacency matrices of the two networks are G_a and G_b respectively. Suppose the two networks are isolated, then the combined adja-

* wvzqbx@hotmail.com

gency matrix is

$$G^0 = \begin{pmatrix} G_a & 0 \\ 0 & G_b \end{pmatrix}, \quad (1)$$

which is a $N \times N$ matrix with $N = N_a + N_b$. There are multiple ways to interconnect the two isolated networks, and the dynamics on the interconnected network relies on the structure of interconnections. The target of the paper is to find the optimal interconnecting strategy such that the spreading prevalence is maximized. After adding the edges, the network become

$$G = G^0 + \delta G, \quad (2)$$

where

$$\delta G = \begin{pmatrix} 0 & G_{ab} \\ G_{ba} & 0 \end{pmatrix} \quad (3)$$

is the adjacency matrix of the interconnections between the two isolated networks. When $(G_{ab})_{ij} = (G_{ba})_{ji} = 1$ for $i \in \{1, \dots, N_a\}$ and $j \in \{1, \dots, N_b\}$, an undirected edge is added between nodes i and j .

For the information spreading dynamics, we adopt the classical susceptible-infected-susceptible (SIS) model. For SIS model, each node can be in either susceptible or recovered state. Initially, a small fraction nodes as seeds (in the infected state), and the remaining nodes in the susceptible state. At each time step, every infected node in network a (b) tries to transmit the information to susceptible neighbors in the same network with probability λ_a (λ_b), and transmits the information to susceptible node in network b (a) with probability λ_{ab} (λ_{ba}). Then all the infected nodes are returned to susceptible state with probability γ_a (γ_b). To investigate the effects of topology on the spreading dynamics directly, we assume that $\lambda_a = \lambda_b = \lambda_{ab} = \lambda_{ba} = \lambda$ and $\gamma_a = \gamma_b$. In the long time limit, the system reaches the stationary state and fraction of infected nodes fluctuates around a stable value. The target of the paper is to choose the interconnecting edge such that the new stable infected density on the interconnected network is maximized.

III. THEORETICAL ANALYSIS

To study the SIS model on networks, we adopt discrete Markovian chain (DMC) approach [49], which assumes that there are no dynamical correlations among the states of neighbors [50]. In this section, we first state the DMC approach of SIS model on network G^0 , when there are no interconnections between networks a and b . Then basing on a perturbation theory of DMC, we deviate a formula that gives the spreading prevalence on the interconnected network approximately. Physical interpretations of this formula are discussed. Finally we study how to find the optimal interconnecting edge basing on the formula.

A. Perturbation theory of the discrete Markovian chain

Let $p_i(t)$ be the probability that node i is in the infected state at time t . Then the node is susceptible with probability $1 - p_i(t)$. The node i is in infected state at $t + 1$ either it is infected at t and does not recovered, or susceptible at t and infected by at least one neighbor. The first case happens with probability $(1 - \gamma)p_i(t)$ and the second with probability $(1 - p_i(t))(1 - q_i(t))$. Here $1 - q_i(t)$ is the probability that node i is infected by at least one neighbor at time t , with

$$q_i(t) = \prod_{j=1}^N [1 - \lambda G_{ij}^0 p_j(t)]. \quad (4)$$

Combining the two cases, the evolution equation of $p_i(t)$ can be written as

$$p_i(t+1) = (1 - \gamma)p_i(t) + (1 - p_i(t))(1 - q_i(t)). \quad (5)$$

In the steady state, we have $p_i(t) = p_i(t+1) = p_i^*$ and $q_i(t) = q_i(t+1) = q_i^*$. Writing the stationary equation of Eqs. (4)-(5) in terms of vectors gives

$$p^* = (1 - \gamma)p^* + (1 - p^*) \cdot (1 - q^*), \quad (6)$$

and

$$q_i^* = \prod_{j=1}^N (1 - \lambda G_{ij}^0 p_j^*), \quad (7)$$

where $p^* = (p_1^*, \dots, p_N^*)^T$, $q^* = (q_1^*, \dots, q_N^*)^T$. The expected number of infected nodes in the stationary state is

$$\mathcal{P} = N^{-1} \mathbf{1}^T p^*. \quad (8)$$

Previous studies [45, 49] revealed that the global epidemic outbreaks when the effective transmission probability $\lambda^* = \lambda/\gamma$ is larger than the leading eigenvalue $1/\omega_1$ of adjacency matrix G^0 , i.e., the epidemic outbreak threshold is $\lambda_c^* = 1/\omega_1$. When $\lambda_c^* \leq 1/\omega_1$ no outbreaks will be observed.

For real world systems, the two networks can be interconnected by some edges. Obviously the epidemic outbreak size will increase after those interconnections are added between the two networks. How much that those interactions will affect the outbreak size? We now use a perturbation theory to get an approximation value.

When adding some interconnections between the two networks, the adjacency matrix become $G = G^0 + \delta G$, the fixed points of the new system should stay close to p^* . Specifically, if start iterating the DMC on the perturbed network with initial condition $p(0) = p^*$, then we can decompose as $p(t) = p^* + \delta p(t)$ and $q(t) = q^* + \delta q(t)$ for some small $\delta p(t)$ and $\delta q(t)$. Then $p(t)$ and $q(t)$ are iterated with Eqs. (4)-(5) by replacing G^0 with G . Writing explicitly, Eq. (5) becomes

$$p^* + \delta p(t+1) = (1 - \gamma)(p^* + \delta p(t)) + (1 - p^* - \delta p(t)) \cdot (1 - q^* - \delta q(t)). \quad (9)$$

Since we only add an edge between two networks, we assume $\delta p(t)$ and $\delta q(t)$ are small, expand Eq. (9) and ignore the second order term, and apply the relation Eq. (6) gives

$$\delta p(t+1) = (q^* - \gamma)\delta p(t) - (1 - p^*) \cdot \delta q(t). \quad (10)$$

In a similar way, now consider Eq. (4) the shifted evolution equation is

$$q_i^* + \delta q_i(t) = \prod_{j=1}^N (1 - \lambda(G_{ij}^0 + \delta G_{ij})(p_j^* + \delta p_j(t))). \quad (11)$$

We can further split the r.h.s. of Eq. (11) by the contributions from G^0 and δG . Note that $G_{ij}^0 = 1$ and $\delta G_{ij} = 1$ can not be observed simultaneously under the setup of the model, thus we can write

$$\begin{aligned} q_i^* + \delta q_i(t) &= \prod_{j=1}^N (1 - \lambda G_{ij}^0 (p_j^* + \delta p_j(t))) \\ &\quad \times \prod_{j=1}^N (1 - \lambda \delta G_{ij} (p_j^* + \delta p_j(t))). \end{aligned} \quad (12)$$

Divide by q_i^* for both sides and substitute Eq. (7) gives

$$\begin{aligned} 1 + \frac{\delta q_i(t)}{q_i^*} &= \prod_{j=1}^N \left(1 - \frac{\lambda G_{ij}^0 \delta p_j(t)}{1 - \lambda G_{ij}^0 p_j^*}\right) \\ &\quad \times \prod_{j=1}^N \left(1 - \frac{\lambda \delta G_{ij} \delta p_j(t)}{1 - \lambda \delta G_{ij} p_j^*}\right) \prod_{j=1}^N (1 - \lambda \delta G_{ij} p_j^*). \end{aligned} \quad (13)$$

Note that the following relation holds

$$\frac{\lambda G_{ij}^0 \delta p_j(t)}{1 - \lambda G_{ij}^0 p_j^*} = G_{ij}^0 \frac{\lambda \delta p_j(t)}{1 - \lambda p_j^*}, \quad (14)$$

since $G_{ij}^0 \in \{0, 1\}$ and similarly when replacing G_{ij}^0 by $\delta G_{ij} \in \{0, 1\}$. Take the logarithm on both sides of Eq. (13), expand to the first orders of $\delta p_i(t)$, $\delta q_i(t)$, and apply the above relation gives

$$\begin{aligned} \frac{\delta q_i(t)}{q_i^*} &= - \sum_{j=1}^N G_{ij}^0 \frac{\lambda \delta p_j(t)}{1 - \lambda p_j^*} - \sum_{j=1}^N \delta G_{ij} \frac{\lambda \delta p_j(t)}{1 - \lambda p_j^*} \\ &\quad + \sum_{j=1}^N \log(1 - \lambda \delta G_{ij} p_j^*). \end{aligned} \quad (15)$$

Again the terms in the last summation can be checked satisfying

$$\log(1 - \lambda \delta G_{ij} p_j^*) = \delta G_{ij} \log(1 - \lambda p_j^*). \quad (16)$$

Definite $N \times N$ diagonal matrix Z with elements

$$Z_{ij} = \delta_{ij} \frac{1}{1 - \lambda p_j^*}. \quad (17)$$

Eq. (15) can be written in matrix form

$$\begin{aligned} \delta q(t) &= - \lambda q^* \circ (G^0 + \delta G) Z \delta p(t) \\ &\quad + q^* \circ \delta G \log(1 - \lambda p^*), \end{aligned} \quad (18)$$

where $\log(1 - \lambda p^*)$ is the vector by taking logarithm of each component of $1 - \lambda p^*$, and \circ denotes component-wise product of vectors. Substitute it back into Eq. (10) gives the following iteration formula for $\delta p(t)$

$$\begin{aligned} \delta p(t+1) &= (q^* - \gamma)\delta p(t) \\ &\quad + (1 - p^*) \circ \lambda q^* \circ (G^0 + \delta G) Z \delta p(t) \\ &\quad - (1 - p^*) \circ q^* \circ \delta G \log(1 - \lambda p^*). \end{aligned} \quad (19)$$

The equation can be written in terms of matrix multiplications

$$\delta p(t+1) = X \delta p(t) + y \quad (20)$$

where

$$X = \lambda \text{diag}(q^* - p^* \circ q^*) (G^0 + \delta G) Z + \text{diag}(q^* - \gamma), \quad (21)$$

and

$$y = -(1 - p^*) \circ q^* \circ \delta G \log(1 - \lambda p^*). \quad (22)$$

Here $\text{diag}(\cdot)$ denotes the diagonal matrix with the input vector as diagonal entries. The stationary solution δp^* on the perturbed system satisfies

$$\delta p^* = X \delta p^* + y, \quad (23)$$

which gives

$$\delta p^* = (\mathbb{I} - X)^{-1} y. \quad (24)$$

This gives an explicit relation between the interconnection edges and shift of stationary infected probabilities. Therefore the target is to choose δG such that the increment of the density of infected nodes

$$\delta \mathcal{P} := N^{-1} \mathbf{1}^T \delta p = N^{-1} \mathbf{1}^T (\mathbb{I} - X)^{-1} y \quad (25)$$

is maximized.

B. Physical interpretations

Before optimizing Eq. (25), we explore the physical interpretations of the strategy, and explain the intuitions behind it. After adding some interconnection edge, we start with $\delta p = 0$ and iterate with the formula Eq. (20) for t steps, then

$$\delta p(t) = (X^{t-1} + X^{t-2} + \dots + X + \mathbb{I}) y, \quad (26)$$

where X^t is the matrix multiplication of X for t times. In fact in the large time limit we have the following expansion

$$(\mathbb{I} - X)^{-1} = \mathbb{I} + X + X^2 + \dots. \quad (27)$$

It appears $\mathbf{1}^T (\mathbb{I} - X)^{-1}$ have a very similar structure to the Katz centrality [51]. Recall the Katz centrality S_{Katz} is defined as

$$S_{\text{Katz}} = \mathbf{1}^T (\mathbb{I} - \beta G)^{-1}, \quad (28)$$

which is by considering numbers of weighted walks between nodes with β the attenuation factor of walk length. Now we show that $\mathbf{1}^T (\mathbb{I} - X)^{-1}$ can be understood as a generalized version of Katz centrality, which further incorporates the dynamical information of the spreading.

When the transmission probability below the epidemic threshold, we have $p^* \approx 0$ and $q^* \approx 1$, then $X \approx 1 - \gamma + \lambda G$ and

$$(\mathbb{I} - X)^{-1} \approx \gamma^{-1} \left(\mathbb{I} - \frac{\lambda}{\gamma} G \right)^{-1}. \quad (29)$$

This is exactly the Katz matrix with $\beta = \lambda/\gamma$ (up to some constant factors). When the spreading rate becomes larger and p^* deviates from 0, the matrix elements of X is given by

$$X_{ij} = G_{ij} \frac{(1 - p_i^*) q_i^*}{1 - \lambda p_j^*}. \quad (30)$$

This is an decreasing function of p_i^* and increasing function of q_i^*, p_j^* . In other words, when above epidemic threshold, $\mathbf{1}^T (\mathbb{I} - X)^{-1}$ can be understood as a weighted version of Katz centrality. The weights favor those edges that are lowly infected in one end (small q_i^*) and its neighborhood (large q_i^*), but in the other end connecting a highly infected node (large p_j^*). Similarly we can see that y_i is an decreasing function of p_i^* and increasing function of q_i^*, p_j^* . Then the matrix inverse is by summing over paths with edges weighted by the dynamical information. Together the optimal strategy can be understood as selecting an edge that connecting high infected nodes to less effected regions of the network. This is consist with the intuition of what should be done to promote the spreading. For the discussions above, we will later refer to the method proposed in this section as *dynamical Katz method*.

C. Choosing the optimal edge

Now we start to discuss how to optimize Eq. (25). First we introduce some notations that will be used later. For the vector p^* , let its part corresponding to network a be p_a^* . Specifically p_a^* is a vector of length N_a with elements

$$(p_a^*)_i = (p^*)_i \quad (31)$$

for $1 \leq i \leq N_a$. Analogously define p_b^* to be the network b part of p^* , also q_a^*, q_b^* for q^* and y_a, y_b for y . Define the $N_a \times N_a$ diagonal matrix Z_a

$$(Z_a)_{ik} = \delta_{ik} \frac{1}{1 - \lambda (p_a^*)_i} = Z_{ik}, \quad (32)$$

for $1 \leq i, k \leq N_a$, and Z_b corresponds to the network b .

Decompose X as $X = X^0 + \delta X$, where

$$X^0 = \lambda \text{diag}(q^* - p^* \circ q^*) G^0 Z + \text{diag}(q^* - \gamma) \quad (33)$$

depends only on G^0 , and

$$\delta X = \lambda \text{diag}(q^* - p^* \circ q^*) \delta G Z \quad (34)$$

only on δG . Note that X^0 is a diagonal block matrix, which can be further written as

$$X^0 = \begin{pmatrix} X_a^0 & 0 \\ 0 & X_b^0 \end{pmatrix}, \quad (35)$$

where X_a^0 is the block diagonal part of X^0 that only depends on G_a

$$X_a^0 = \lambda \text{diag}(q_a^* - p_a^* \circ q_a^*) G_a Z_a + \text{diag}(q_a^* - \gamma), \quad (36)$$

and similarly for X_b^0

$$X_b^0 = \lambda \text{diag}(q_b^* - p_b^* \circ q_b^*) G_b Z_b + \text{diag}(q_b^* - \gamma). \quad (37)$$

Meanwhile δX is an off-diagonal block matrix

$$\delta X = \begin{pmatrix} 0 & \delta X_{ab} \\ \delta X_{ba} & 0 \end{pmatrix}, \quad (38)$$

with the off-diagonal blocks given by

$$\begin{aligned} \delta X_{ab} &= \lambda \text{diag}(q_a^* - p_a^* \circ q_a^*) G_{ab} Z_b \\ \delta X_{ba} &= \lambda \text{diag}(q_b^* - p_b^* \circ q_b^*) G_{ba} Z_a. \end{aligned} \quad (39)$$

Using the properties of block matrices, the matrix inverse in Eq. (24) can be written as

$$\begin{aligned} (\mathbb{I} - X)^{-1} &= \begin{pmatrix} \mathbb{I} - X_a^0 & -\delta X_{ab} \\ -\delta X_{ba} & \mathbb{I} - X_b^0 \end{pmatrix}^{-1} \\ &= \begin{pmatrix} C & C \delta X_{ab} B \\ D \delta X_{ba} A & D \end{pmatrix}, \end{aligned} \quad (40)$$

where

$$A = (\mathbb{I} - X_a^0)^{-1}, \quad B = (\mathbb{I} - X_b^0)^{-1} \quad (41)$$

and

$$\begin{aligned} C &= (\mathbb{I} - X_a^0 - \delta X_{ab} B \delta X_{ba})^{-1}, \\ D &= (\mathbb{I} - X_b^0 - \delta X_{ba} A \delta X_{ab})^{-1}. \end{aligned} \quad (42)$$

Now consider the case when adding only one interconnecting edge, say between node i of network a and node j of b . Then the matrix $G_{ab} = G_{ba}^T$ can be written as an outer product

$$G_{ab} = uv^T, \quad (43)$$

where u is a vector of length N_a with $u_k = \delta_{k,i}$ for $1 \leq k \leq N_a$, and v a length N_b vector with $v_k = \delta_{k,j}$ for $1 \leq k \leq N_b$. Define short notations as

$$x_{ij} := \lambda [(q_a^*)_i - (p_a^*)_i (q_a^*)_i] [1 - \lambda (p_b^*)_j]^{-1}, \quad (44)$$

$$x_{ji} := \lambda [(q_b^*)_j - (p_b^*)_j (q_b^*)_j] [1 - \lambda (p_a^*)_i]^{-1},$$

then it's easy to check that

$$\delta X_{ab} = x_{ij}uv^T, \delta X_{ba} = x_{ji}vu^T. \quad (45)$$

Thus

$$\delta X_{ab}B\delta X_{ba} = x_{ij}x_{ji}B_{jj}uu^T \quad (46)$$

In other words, $\delta X_{ab}B\delta X_{ba}$ is an all-zero matrix except in the j th element in the diagonal. The Sherman-Morrison formula says that

$$\begin{aligned} C &= (\mathbb{I} - X_a^0 - x_{ij}x_{ji}B_{jj}uu^T)^{-1} \\ &= A + \frac{x_{ij}x_{ji}B_{jj}Auu^T A}{1 - x_{ij}x_{ji}A_{ii}B_{jj}}. \end{aligned} \quad (47)$$

With the formula we can construct $(\mathbb{I} - X)^{-1}$ easily from C . Similarly,

$$\begin{aligned} D &= (\mathbb{I} - X_b^0 - x_{ij}x_{ji}A_{ii}vv^T)^{-1} \\ &= B + \frac{x_{ij}x_{ji}A_{ii}Bvv^T B}{1 - x_{ij}x_{ji}A_{ii}B_{jj}}. \end{aligned} \quad (48)$$

Again define short notations for convenience,

$$\begin{aligned} c_{ij} &= -[(q_a^*)_i - (p_a^*)_i (q_a^*)_i] \log [1 - \lambda (p_b^*)_j], \\ c_{ji} &= -[(q_b^*)_j - (p_b^*)_j (q_b^*)_j] \log [1 - \lambda (p_a^*)_i], \end{aligned} \quad (49)$$

and y_a, y_b can be checked satisfying

$$y_a = c_{ij}u, y_b = c_{ji}v. \quad (50)$$

Combine the above computations, we can have a final formula for

$$N\delta\mathcal{P} = \mathbf{1}^T C y_a + \mathbf{1}^T C \delta X_{ab} B y_b + \mathbf{1}^T D y_b + \mathbf{1}^T D \delta X_{ba} A y_a. \quad (51)$$

This first term on the r.h.s. can be written as

$$\begin{aligned} \mathbf{1}^T C y_a &= \mathbf{1}^T A y_a + \frac{x_{ij}x_{ji}B_{jj}}{1 - x_{ij}x_{ji}A_{ii}B_{jj}} (\mathbf{1}^T A)_i u^T A y_a \\ &= \frac{c_{ij}}{1 - x_{ij}x_{ji}A_{ii}B_{jj}} (\mathbf{1}^T A)_i, \end{aligned} \quad (52)$$

where the first line is by substituting Eq. (47), and second line is by using definition of y_a and u . For the second term in Eq. (51)

$$\begin{aligned} \mathbf{1}^T C \delta X_{ab} B y_b &= c_{ji}x_{ij}B_{jj}\mathbf{1}^T C u \\ &= \frac{c_{ji}x_{ij}B_{jj}}{1 - x_{ij}x_{ji}A_{ii}B_{jj}} (\mathbf{1}^T A)_i. \end{aligned} \quad (53)$$

With similar computations, we can obtain the rest two terms of Eq. (51), which are

$$\mathbf{1}^T D y_b = \frac{c_{ji}}{1 - x_{ij}x_{ji}A_{ii}B_{jj}} (\mathbf{1}^T B)_j, \quad (54)$$

and

$$\mathbf{1}^T D \delta X_{ba} A y_a = \frac{c_{ij}x_{ji}A_{ii}}{1 - x_{ij}x_{ji}A_{ii}B_{jj}} (\mathbf{1}^T B)_j. \quad (55)$$

Combine the above computations we have

$$\begin{aligned} N\delta\mathcal{P} &= \frac{c_{ij} + c_{ji}x_{ij}B_{jj}}{1 - x_{ij}x_{ji}A_{ii}B_{jj}} (\mathbf{1}^T A)_i + \\ &+ \frac{c_{ji} + c_{ij}x_{ji}A_{ii}}{1 - x_{ij}x_{ji}A_{ii}B_{jj}} (\mathbf{1}^T B)_j. \end{aligned} \quad (56)$$

This gives a simple formula connecting the interconnecting edge and the stationary infected density. The optimal strategy is just to select the edge with highest corresponding $\delta\mathcal{P}$. Obviously, the strategy not only relies on the network topology (i.e., the adjacency matrices G_a and G_b), but also on the dynamical information of the spreading process when the two networks are isolated (i.e., λ , γ and p^*).

IV. NUMERICAL SIMULATIONS

In this section, we perform extensive numerical simulations on both synthetic and real world networks to verify the performance of the strategy. Note that we do not compare the DMC predictions with Monte Carlo simulations since the DMC approach can well predict the simulations [49].

For two given networks with node numbers N_a and N_b , there are in total $M_l = N_a \times N_b$ latent interconnections. For small networks it is possible to exhaustively check all the latent connections to find the optimal one. When N becomes large, exhaustive searching becomes computational slow and gradually impossible due to high computational complexity. Next we first use small networks to check the accuracy of $\delta\mathcal{P}$ predicted by Eq. (56), and compare the optimal edge proposed by the strategy to the exact optimal one.

To build synthetic networks, we adopt the uncorrelated configuration model with power-law degree distributions. Specifically, we set the degree distributions of network a and b as $P(k) \sim k^{-\alpha_a}$ and $P(k) \sim k^{-\alpha_b}$ respectively, where α_a and α_b are the degree exponents. The network sizes considered are $N_a = N_b = 100$. Without lose of generality, we set the recovery probability of SIS model to $\gamma = 0.5$, with the infection probability λ as a tuning parameter.

We first compare $\delta\mathcal{P}$ predicted by Eq. (56) with the exact theoretical predictions from DMC approach. Let $\delta\mathcal{P}^{\text{approx}}$ be the approximate $\delta\mathcal{P}$ predicted by Eq. (56) and let $\delta\mathcal{P}^{\text{exact}}$ be the exact value. For each latent edge connecting node $i \in \{1, \dots, N_a\}$ and node $j \in \{1, \dots, N_b\}$, we compute $\delta\mathcal{P}^{\text{approx}}$ using Eq. (56) for $\lambda = 0.3$ (Fig. 1(a)) and $\lambda = 0.5$ (Fig. 1(c)). Then we add the edge to the network and iterate the DMC to get $\delta\mathcal{P}^{\text{exact}}$ which are shown in Fig. 1(b) and Fig. 1(d) for $\lambda = 0.3$ and $\lambda = 0.5$ respectively. In Fig. 1(a) and Fig. 1(b) the nodes are arranged in identical order, and also for Fig. 1(c) and Fig. 1(d). The approximate values seem usually higher than the exact ones, but intuitively they are strongly correlated. The maximum relative error $(\delta\mathcal{P}^{\text{approx}} - \delta\mathcal{P}^{\text{exact}}) / \delta\mathcal{P}^{\text{exact}}$ for all edges is 0.315 in

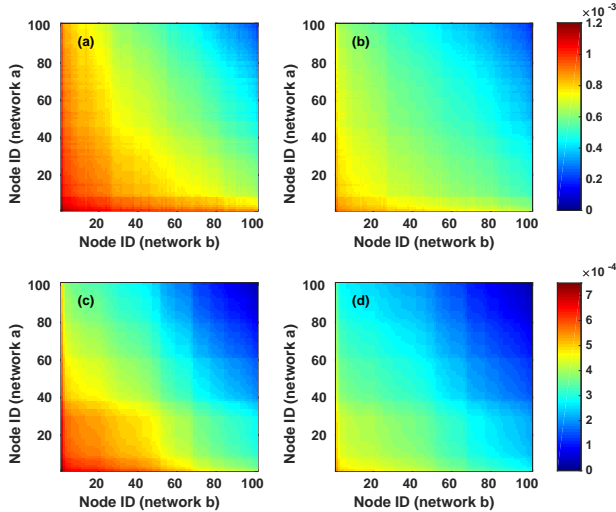


FIG. 1. (Color online) The increment $\delta\mathcal{P}$ in the expected density of infected nodes in the stationary state for all latent interconnections. The vertical and horizontal axes correspond to the ID of nodes in two networks. Thus each point correspond to an edge connecting network a and network b , and its color denotes the value of $\delta\mathcal{P}$. (a) The approximate and (b) theoretical predictions of $\delta\mathcal{P}$ with $\lambda = 0.3$. (c) The approximate and (d) theoretical predictions of $\delta\mathcal{P}$ with $\lambda = 0.5$. The nodes are arranged in identical orders for (a) and (b) and same for (c) and (d). Other parameters are set to be $N_a = N_b = 100$, $\alpha_a = 2.3$, $\alpha_b = 3.0$ and $\gamma = 0.5$.

Fig. 1(a-b), and 0.396 in Fig. 1(c-d). However we will show that they are almost linearly correlated, which suggests the approximate value is sufficient to give the optimal edge.

To see the correlations, we compute the Spearman's rank correlation coefficient [34, 52] of the approximate and exact $\delta\mathcal{P}$. Consider scoring all the latent interconnecting edges by $\delta\mathcal{P}^{\text{exact}}$ and $\delta\mathcal{P}^{\text{approx}}$, then we can obtain two rankings of the edges. Let r_{ij} and r'_{ij} be the rank of the edge connecting node i in network a and node j in network b scored by $\delta\mathcal{P}^{\text{exact}}$ and $\delta\mathcal{P}^{\text{approx}}$ respectively. Spearman's rank correlation coefficient is defined as

$$m_s = 1 - 6 \frac{\sum_{i=1}^{N_a} \sum_{j=1}^{N_b} (r_{ij} - r'_{ij})^2}{M_l(M_l^2 - 1)}. \quad (57)$$

We plot m_s as a function of λ in Fig. 2 by the blue circles. It can be observed that Spearman's rank correlation coefficients are very close to 1 for all λ . The minimum value of m_s for all λ in Fig. 2 is 0.9968. This suggests that the proposed strategy predicts the overall order of $\delta\mathcal{P}^{\text{exact}}$ accurately.

Apart from the overall strong correlations for the approximate and exact values of $\delta\mathcal{P}$ in rank, we are more concerned with how it is behaved for the top ranked edge. We further verify the performance of the strategy by comparing the predicted optimal edge to the true optimal one. For each λ , we select the edge with highest $\delta\mathcal{P}^{\text{approx}}$ predicted by the dynamical Katz method, and compute its rank in all the latent edges scored by the exact $\delta\mathcal{P}^{\text{exact}}$. The normalized edge rank (rank

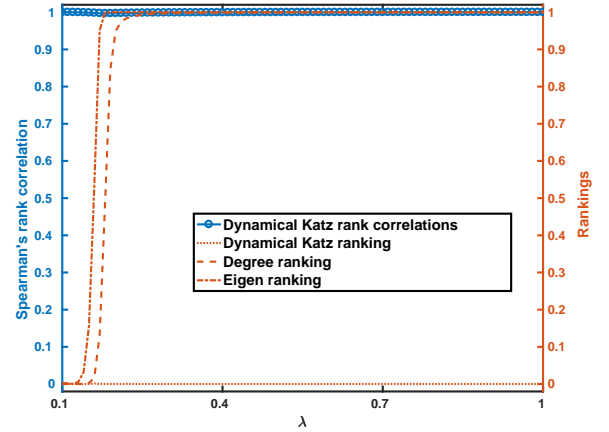


FIG. 2. (Color online) Performances of different strategies versus transmission probability. Spearman's rank correlation coefficient m_s between rank predicted by the dynamical Katz method and the accurate ranking order versus λ is given by the blue circles. The ranks scored by exact $\delta\mathcal{P}$ of the optimal edge given by dynamical Katz, degree and engenvector are denoted by the orange dotted, dashed and dash-dot lines respectively. Note that since when below the spreading threshold, the prevalence \mathcal{P} is zero and makes the rankings trivial, we consider λ starting slightly above the threshold. Other parameters are set to be $N_A = N_B = 100$, $\gamma_A = 3.0$, $\gamma_B = 2.3$. and $\gamma = 0.5$.

divided by $M_l = N_a \times N_b$) is shown in Fig. 2 by the orange dotted line. It can be seen that the normalized edge rank is very close to 0 for all values of λ . It's not easy to distinguish visually but for most values of λ the optimal edge predicted by the strategy coincide with the true one (with normalized rank $1/M_l$).

As the dynamical Katz method incorporate both the information of the network structure and spreading process, it is useful to compare with simple strategies that only consider the static structures of networks to understand how the information of dynamics play the role. Specifically we consider the strategies of connecting the two nodes with highest degree or the highest eigenvector centralities. The normalized ranks of the two static strategies are shown in Fig. 2 by the orange dashed and dash-dot lines. These two strategies are optimal or close to optimal when transmission probability λ is slightly above its critical value, but fails quickly when λ becomes large.

As discussed in Sce. III B, when $p^* \approx 0$, the dynamical Katz matrix reduces to Katz matrix. When λ/γ is small, approximately we have

$$(\mathbb{I} - X)^{-1} \approx \gamma^{-1}\mathbb{I} + \lambda G \quad (58)$$

and this reduces to the degree centrality. For uncorrelated configuration model, degree and eigenvector centrality are strongly correlated. When λ is small, these nodes with high values of centralities (e.g., degree and eigenvector centrality) have larger probabilities to be infected. Once we build an connection between with them, these nodes together with their

neighbors will form an infected cluster [53], and further transmit the infection to the remaining nodes. Thus in this region of λ , the degree and eigenvector strategies perform well. For large values of λ , the epidemic globally outbreaks and nodes with small centralities have larger probabilities not to be infected. In this case, we need to build additional connections to those nodes for promoting the spreading dynamics. Therefore, both the degree and eigenvector strategies fails and the information of dynamics has to be taken into consideration.

For large networks, exhaustive searching becomes impossible. In this case we compare the performance of the dynamical Katz method with the two heuristic methods based on degree and eigenvector centralities. For the three strategies, we add the predicted optimal edge to the network respectively and compare their resulting $\delta\mathcal{P}$. First still we consider synthetic networks. We build three pairs of networks with power-law degree distributions, with degree exponents (i) $\alpha_a = 2.3$ and $\alpha_b = 3.0$, (ii) $\alpha_a = 3.0$ and $\alpha_b = 3.0$, (iii) $\alpha_a = 4.0$ and $\alpha_b = 3.0$. $\delta\mathcal{P}$ versus λ are shown in Fig. 3. When λ is close to the critical point, all the three strategies give very close performance. As discussed above, this should also close to the optimal value of $\delta\mathcal{P}$. When λ becomes large, dynamical Katz outperforms the other two heuristic ones for all the three pairs of networks with different degree exponents. In this case, connecting large degree or eigenvector centrality nodes gives almost zero marginal improvement in $\delta\mathcal{P}$, and dynamical Katz is better about three orders of magnitude. Moreover, it is worth noticing that $\delta\mathcal{P}$ is always maximized when slightly above the spreading threshold, which suggests that the marginal improvement is optimized when near the critical point.

Now we test the dynamical Katz method on real-world networks. Three pairs of networks are considered, which are (i) Advogato [54] and Facebook [55], (ii) OpenFlights [56] and Air traffic control [56], (iii) Adolescent health [57] and Physicians [58]. Here the first pair (Advogato and Facebook) are two online social networks, the second pair (OpenFlights and Air traffic control) are infrastructure networks of airports and flights. The third pair (Adolescent health and Physicians) are two offline social networks. The networks are downloaded from [56] and detailed introductions to these networks can be found therein. Some basic statistics of the six real-world networks are shown in TABLE I.

$\delta\mathcal{P}$ versus λ for the three pairs of real word networks are shown in Fig. 4. As for the synthetic networks, we can see that dynamical Katz method performs best for all values of λ . Still for small λ the three methods are quite close. For larger λ , the dynamical Katz gives significant improvements compared to the other two (usually for several orders of magnitude), which further confirmed the effectiveness of our method.

V. DISCUSSION

In the paper we have studied the problem of finding the optimal interconnecting edge for promoting spreading dynamics. Based on a perturbation theory of the DMC, we obtain a Katz-like index to predict the spreading prevalence on the

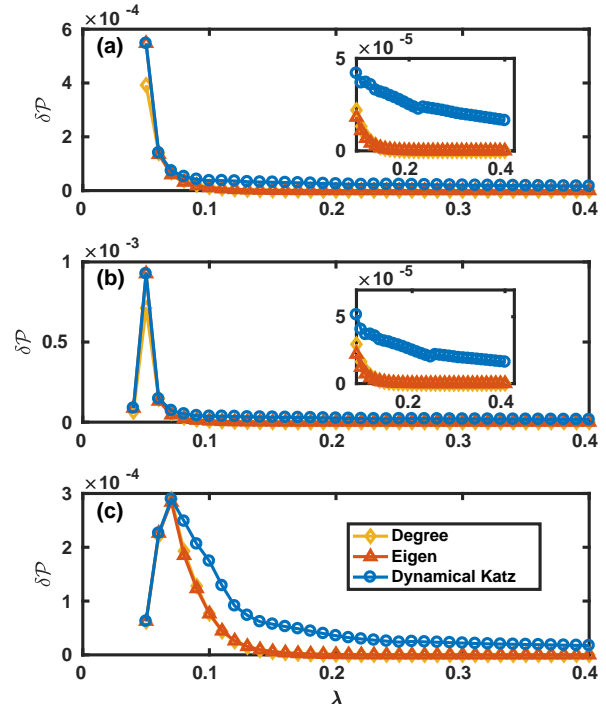


FIG. 3. (Color online) The increment $\delta\mathcal{P}$ of the density of infected nodes in the stationary state when adding one interconnecting edge. $\delta\mathcal{P}$ versus λ on synthetic networks with power law degree exponents (a) $\alpha_a = 2.3$ and $\alpha_b = 3.0$, (b) $\alpha_a = 3.0$ and $\alpha_b = 3.0$, (c) $\alpha_a = 4.0$ and $\alpha_b = 3.0$ are plotted. In (a) and (b), $\delta\mathcal{P}$ are close for different strategies when λ is large, thus $\delta\mathcal{P}$ versus λ in this region are shown in the insets for visual purpose. Again the lines correspond to degree and eigenvector centrality might be highly overlapped to distinguish. Still we consider λ start slightly above the spreading threshold to avoid the trivial cases. Other parameters are set to be $N_A = N_B = 5000$ and $\gamma = 0.5$.

interconnected networks. This index predicts accurately the optimal interconnecting edge for better spreading over all parameter regions as tested on small networks. For large synthetic and real world networks, the method outperforms some heuristic strategies like connecting large degree or eigenvector centrality nodes. When λ is small, the three strategies give close performance, but for large λ , our method improves the two heuristic ones by several orders of magnitude. Apart from the accuracy in predicting the optimal edge, the dynamical Katz method also has a clear physical interpretation of how the optimal edge is chosen.

As we only consider adding one interconnecting edge here, real world multilayer networks usually have multiple interconnecting edges. Note that Eq. (25) which connects the interconnections and spreading prevalence works for general interconnecting structures. This could possibly provide a starting point for optimizing over multiple edges. As in the paper we consider adding only one edge, the interconnection structure matrix C can be written as an outer product of two vec-

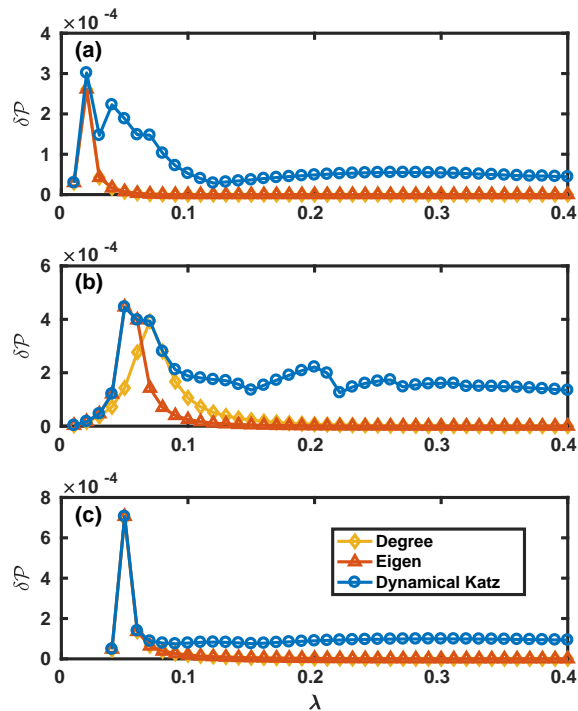


FIG. 4. (Color online) The increment $\delta\mathcal{P}$ of the density of infected nodes in the stationary state when adding one interconnecting edge. $\delta\mathcal{P}$ versus λ on for real world networks (a) Advogato and Facebook , (b) OpenFlights and Air traffic control, (c) Adolescent health and Physicians. Data for degree and eigenvector method are highly overlapped.

TABLE I. Some basic statistics of six real-world networks. The statistics includes the number of nodes (N), number of edges (M), maximal degree (k_{\max}), first ($\langle k \rangle$) and second ($\langle k^2 \rangle$) moments of the degree distribution and the theoretical spreading threshold predicted by discrete Markov chain $\lambda_c^* = 1/\omega_1$.

	N	M	k_{\max}	$\langle k \rangle$	$\langle k^2 \rangle$	λ_c^*
Advogato	5042	39227	803	15.56	1284.00	0.014
Facebook	2888	2981	769	2.06	528.13	0.036
OpenFlights	2905	15645	242	10.77	601.45	0.016
Air traffic control	1226	2408	34	3.928	28.90	0.109
Adolescent health	2539	10455	27	8.24	86.41	0.076
Physicians	117	465	26	7.95	79.16	0.099

tors. By applying the Sherman-Morrison formula, $\delta\mathcal{P}$ can be converted to a simple form that is easy to optimize. When consider adding multiple edges, the outer product decomposition of C does not work in general. How to find a simple way to optimize Eq. (25) in this case is not clear yet. Moreover, the perturbation method developed in the paper could also be extended to other types of networks (e.g., temporal networks) and spreading models (e.g., social contagions and cascading failures).

ACKNOWLEDGMENTS

This work was partially supported by National Natural Science Foundation of China (Nos. 61433014 and 61673086), China Postdoctoral Science Foundation (Grant No. 2018M631073) and Fundamental Research Funds for the Central Universities.

- [1] L. Lü, D. Chen, X.-L. Ren, Q.-M. Zhang, Y.-C. Zhang, and T. Zhou, *Physics Reports* **650**, 1 (2016).
- [2] M. Kitsak, L. K. Gallos, S. Havlin, F. Liljeros, L. Muchnik, H. E. Stanley, and H. A. Makse, *Nature Physics* **6**, 888 (2010).
- [3] F. Morone and H. A. Makse, *Nature* **524**, 65 (2015).
- [4] L. Lü, T. Zhou, Q.-M. Zhang, and H. E. Stanley, *Nature Communications* **7**, 10168 (2016).
- [5] W. Chen, Y. Wang, and S. Yang, in *Proceedings of the 15th ACM SIGKDD International Conference on Knowledge Discovery and Data Mining* (ACM, 2009) pp. 199–208.
- [6] W. Chen, C. Wang, and Y. Wang, in *Proceedings of the 16th ACM SIGKDD International Conference on Knowledge Discovery and Data Mining* (ACM, 2010) pp. 1029–1038.
- [7] F. Morone, B. Min, L. Bo, R. Mari, and H. A. Makse, *Scientific Reports* **6**, 30062 (2016).
- [8] Y. Hu, S. Ji, Y. Jin, L. Feng, H. E. Stanley, and S. Havlin, *Proceedings of the National Academy of Sciences*, 201710547 (2018).
- [9] S. Ji, L. Lü, C. H. Yeung, and Y. Hu, *New Journal of Physics* **19**, 073020 (2017).
- [10] Z.-M. Ren, A. Zeng, D.-B. Chen, H. Liao, and J.-G. Liu, *Europhysics Letters* **106**, 48005 (2014).
- [11] H. Liao, M. S. Mariani, M. Medo, Y.-C. Zhang, and M.-Y. Zhou, *Physics Reports* **689**, 1 (2017).
- [12] S. Pei and H. A. Makse, *Journal of Statistical Mechanics: Theory and Experiment* **2013**, P12002 (2013).
- [13] D. Chen, L. Lü, M.-S. Shang, Y.-C. Zhang, and T. Zhou, *Physica A* **391**, 1777 (2012).
- [14] Y. Liu, M. Tang, Y. Do, and P. M. Hui, *Physical Review E* **96**, 022323 (2017).
- [15] R. Yang, T. Zhou, Y.-B. Xie, Y.-C. Lai, and B.-H. Wang, *Physical Review E* **78**, 066109 (2008).
- [16] L. Gao, W. Wang, L. Pan, M. Tang, and H.-F. Zhang, *Scientific Reports* **6**, 38220 (2016).
- [17] R. Yang, L. Huang, and Y.-C. Lai, *Physical Review E* **78**, 026111 (2008).
- [18] F. Roshani and Y. Naimi, *Physical Review E* **85**, 036109 (2012).
- [19] L. Gao, W. Wang, P. Shu, H. Gao, and L. A. Braunstein, *Europhysics Letters* **118**, 18001 (2017).
- [20] P.-B. Cui, W. Wang, S.-M. Cai, T. Zhou, Y.-C. Lai, *Physical Review E* **98**, 052311 (2018).
- [21] J. Aguirre, D. Papo, and J. M. Buldú, *Nature Physics* **9**, 230 (2013).
- [22] G. Del Ferraro, A. Moreno, B. Min, F. Morone, Ú. Pérez-Ramírez, L. Pérez-Cervera, L. C. Parra, A. Holodny, S. Canals, and H. A. Makse, *Nature Communications* **9**, 2274 (2018).

- [23] A. Milanese, J. Sun, and T. Nishikawa, *Physical Review E* **81**, 046112 (2010).
- [24] P. Van Mieghem, H. Wang, X. Ge, S. Tang, and F. Kuipers, *The European Physical Journal B* **76**, 643 (2010).
- [25] J. Aguirre, R. Sevilla-Escoboza, R. Gutiérrez, D. Papo, and J. Buldú, *Physical Review Letters* **112**, 248701 (2014).
- [26] Y. Li, X. Wu, J.-a. Lu, and J. Lü, *IEEE Transactions on Circuits and Systems II: Express Briefs* **63**, 206 (2016).
- [27] J. Wei, X. Wu, J.-A. Lu, and X. Wei, *Europhysics Letters* **120**, 20005 (2018).
- [28] X. Wei, J. Emenheiser, X. Wu, J.-A. Lu, and R. M. D'Souza, *Chaos* **28**, 013110 (2018).
- [29] Y. Dai, J. Zhang, and W. Wang, *Europhysics Letters* **125**, 18003 (2019).
- [30] P. C. V. da Silva, F. Velásquez-Rojas, C. Connaughton, F. Vazquez, Y. Moreno, and F. A. Rodrigues, *arXiv:1812.01386* (2018).
- [31] M. De Domenico, C. Granell, M. A. Porter, and A. Arenas, *Nature Physics* **12**, 901 (2016).
- [32] C. Granell, S. Gómez, and A. Arenas, *Physical Review Letters* **111**, 128701 (2013).
- [33] C. Granell, S. Gómez, and A. Arenas, *Physical Review E* **90**, 012808 (2014).
- [34] W. Wang, M. Tang, H. Yang, Y. Do, Y.-C. Lai, and G. Lee, *Scientific Reports* **4**, 5097 (2014).
- [35] X. Chen, W. Wang, S. Cai, H. E. Stanley, and L. A. Braunstein, *Journal of Statistical Mechanics: Theory and Experiment* **2018**, 053501 (2018).
- [36] J. Gao, S. V. Buldyrev, H. E. Stanley, and S. Havlin, *Nature Physics* **8**, 40 (2012).
- [37] A. Tejedor, A. Longjas, E. Foufoula-Georgiou, T. T. Georgiou, and Y. Moreno, *Physical Review X* **8**, 031071 (2018).
- [38] W. Wang, M. Cai, and M. Zheng, *Physica A* **499**, 121–128 (2018).
- [39] F. Radicchi and A. Arenas, *Nature Physics* **9**, 717 (2013).
- [40] S. D. Reis, Y. Hu, A. Babino, J. S. Andrade Jr, S. Canals, M. Sigman, and H. A. Makse, *Nature Physics* **10**, 762 (2014).
- [41] P. Van Mieghem, *Physical Review E* **93**, 042305 (2016).
- [42] E. Cozzo, G. F. de Arruda, F. A. Rodrigues, and Y. Moreno, *arXiv:1901.04523* (2019).
- [43] X. Zhang, S. Boccaletti, S. Guan, and Z. Liu, *Physical Review Letters* **114**, 038701 (2015).
- [44] Y. Hu, S. Havlin, and H. A. Makse, *Physical Review X* **4**, 021031 (2014).
- [45] G. F. de Arruda, E. Cozzo, T. P. Peixoto, F. A. Rodrigues, and Y. Moreno, *Physical Review X* **7**, 011014 (2017).
- [46] J. Sanz, C.-Y. Xia, S. Meloni, and Y. Moreno, *Physical Review X* **4**, 041005 (2014).
- [47] A. Saumell-Mendiola, M. Á. Serrano, and M. Boguná, *Physical Review E* **86**, 026106 (2012).
- [48] L. Pan, W. Wang, S. Cai, and Z. Tao, Unpublished (2019).
- [49] S. Gómez, A. Arenas, J. Borge-Holthoefer, S. Meloni, and Y. Moreno, *Europhysics Letters* **89**, 38009 (2010).
- [50] W. Wang, M. Tang, H. E. Stanley, and L. A. Braunstein, *Reports on Progress in Physics* **80**, 036603 (2016).
- [51] M. Newman, *Networks: An introduction* (Oxford University Press, 2010).
- [52] K.-M. Lee, J. Y. Kim, W.-k. Cho, K.-I. Goh, and I. Kim, *New Journal of Physics* **14**, 033027 (2012).
- [53] A. V. Goltsev, S. N. Dorogovtsev, J. Oliveira, and J. F. Mendes, *Physical Review Letters* **109**, 128702 (2012).
- [54] P. Massa, M. Salvetti, and D. Tomasoni, in *Dependable, Autonomic and Secure Computing, 2009. DASC'09. Eighth IEEE International Conference on* (IEEE, 2009) pp. 658–663.
- [55] J. Leskovec and J. J. McAuley, in *Advances in neural information processing systems* (2012) pp. 539–547.
- [56] <http://konect.uni-koblenz.de/>.
- [57] J. Moody, *Social Networks* **23**, 261 (2001).
- [58] J. Coleman, E. Katz, and H. Menzel, *Sociometry* **20**, 253 (1957).